

This illustrates the diffusivity governing the capsules swelling are similar for both cases and the analysis developed by Sherwood *et al* can be used to describe ovalbumin-alginate capsules.

After reaching a new equilibrium, the capsules undergoes renewed inflation until it eventually ruptures after 70 hours. The reason for this secondary phenomena is unknown. It could be related to the rearrangements of the cross-linked bonds in the membrane. Currently this is an open question.

Determining the area dilation modulus of capsules is done by placing capsules at varying salt concentrations and leaving them until they have reached a new equilibrium radius. Examples for stiff and pliable batch of capsules are shown in Figure 3.

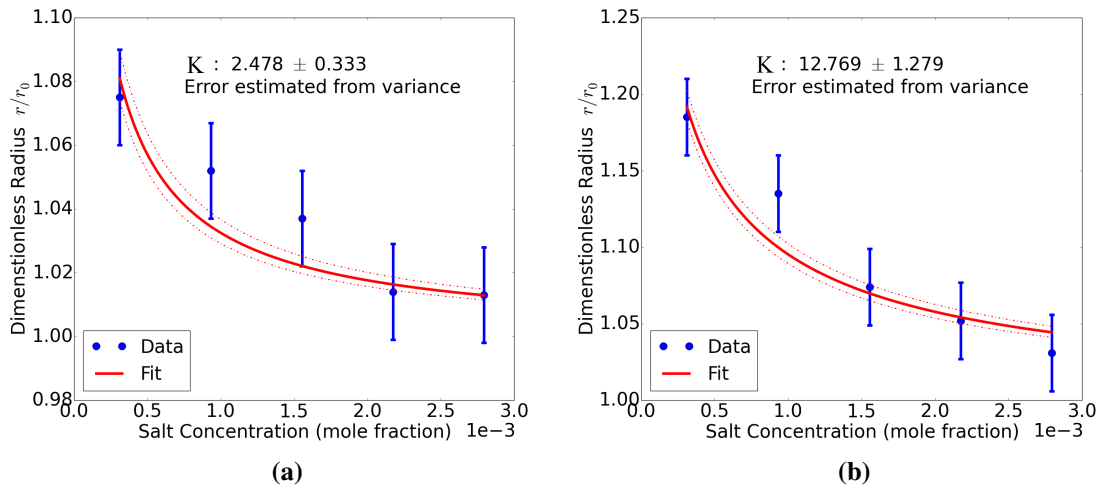


Figure 3: Equilibrium radius of capsules of two batches relative to the radius at 13.5 g/l salt concentration. Note that this method fails to rank these capsules correctly. **a)** Stiff capsules (made with 0.0045 molar alkaline) **b)** Malleable capsules (made with 0.001 molar alkaline).

As can be seen from the comparison, while the method predicts the correct order of magnitude it misjudges the relative elasticity of the two capsule batches. This is caused by a strong dependence on the initial radius r_0 in equation 5 ($K \propto r_0^{-5}$), limiting the practicality of this method.

The inaccuracy of the method mean that this is insufficient to characterise capsules. Considering our interest in the strong deformation of capsules, the use of linear elasticity is an additional constraint.

3.2 Compression

The compression of a capsule between parrallel plates will be explored in this section. The general process used for experiments and the subsequent matching with the theoretical model follows the process employed by Carin *et al* [14].

First, for a given capsule the experiment was carried out, recording the force exerted on the capsule as well as the deformation. This information, along with a best guess for the area shear modulus G_s , is given to the computer program. It then finds the value for G_s for which experimental parameters are matched. This returns a value of G_s for every value supplied to the program.

To determine the correct constitutive law and confirm the functioning of the method,

we assume that the material coefficients should be constant during the whole compression process. This restricts the constitutive laws under consideration to the simplest nonlinear cases. If an appropriate constitutive law has been selected, the value of G_s should be constant throughout compression.

A semi-analytic treatment of the compression of capsules between parallel plates is used, as derived by Feng and Yang [12] and generalized to any constitutive law by Lardner and Pujara [13].

3.2.1 Experimental Implementation

A Instron 3345 Single Column Testing System is used with a 100 N load cell to record the force on and the displacement of the top plate compressing the capsule. The set-up consist of a saline bath through which the top plate is lowered onto an anvil. A schematic is shown in Figure 4 a) next to a typical experimental output.

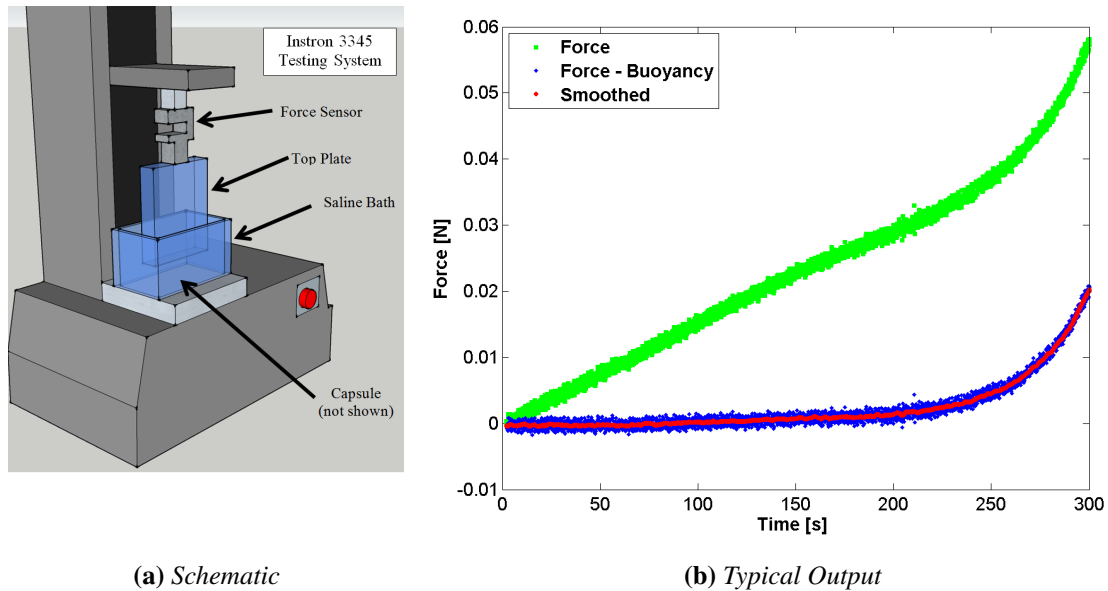


Figure 4: *a) Schematic of the set-up used for the compression. A slender perspex plate is used to compress a capsule in a saline bath. The bath is made out of perspex, allowing pictures of the compression to be take using a still camera. The Instron records the force and the displacement of the top plate. b) A typical example of the force exerted during compression. The top plate is lowered at 0.01 mm/s. The green datat points indicate the force measured and the blue the force after subtracting the buoyancy force exerted on the top plate. The red line is smoothed and used for comparison to the images taken.*

Initially, the force exerted on the top plate due to buoyancy forces is measured as it is lowered through the saline bath without a capsule present. This is then subtracted from subsequent force measurements. The top plate is lowered at a rate of 0.01 mm/s, such that the complete compression takes approximately 5 minutes. This has been chosen so that it is slow enough for the compression to be quasi-static with respect to membrane deformation while at the same time be instantaneous compared to osmotic changes that take place on the time-scale of hours. During the compression, images are taken of the capsule every 2- 3 seconds to match the shape to the compression. The images are calibrated with a ball bearing 4 mm in diameter at the beginning of the experiment. An example of a capsule being compressed is shown in Figure 5.

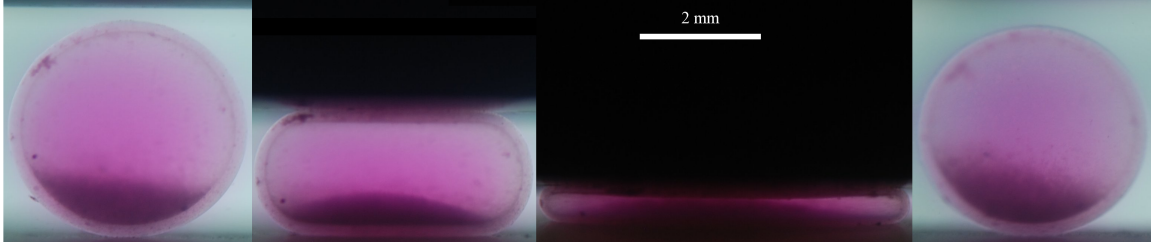


Figure 5: Example of compression of a capsule of diameter 3.7 mm and a membrane thickness that is 10 % of radius, shown at 4 points during the compression. The capsule has been coloured red and time progresses from left to right. Note that the capsule returns to its original shape after the compression.

In 2 out of the 39 compression test carried out the shape of the capsule after compression was measurably different. Upon placing these capsules in saline for 24 hours they regained their previous shape. This semi-permanent deformation is most likely is due to liquid being squeezed out of the capsule in the latest stage of the compression. However, the presence of plastic deformations cannot be excluded in those two cases. Only data from experiments in which the capsule immediately return to its previous shape have been used for further processing.

The uncertainty in force is of the order of 1 mN, as estimated from the precision of the force measurement. On the images, one pixel corresponds to 7 μm . However, due to difficulties to locate the exact boundary, the error on distance measurements is larger, especially at large compression due to the reduced amount of light in the image. The error on the size of the contact area is always less than 0.1mm. This is used to determine the pressure from the force measurement as well as the degree of compression.

The uncertainty on the force measurement is substantially, given that the burst force of the capsules is between 40 and 120 mN. A more accurate force measurement is desirable and in future experiments, 5 N load cell will be used instead of the current 100 N cell.

3.2.2 Equations of Equilibrium

There are three key assumptions in the derivation that follows that of Feng and Yang [12]

1. The profile of both the deformed and undeformed configuration are axis-symmetric
2. The elastic membrane is composed of incompressible homogeneous isotropic material with constant thickness before deformation.
3. The magnitude of the thickness of the membrane before deformation, h , is small compared to the other dimensions meaning that bending resistance is negligible.

For the undeformed configuration, the spherical coordinates (r, θ, ψ) are used and for the deformed configuration the cylindrical coordinates (ρ, θ, η) . This is illustrated in Fig. 6. The governing equations are separately applied to the region in contact with the plate and the free surface. A prim ' indicates differentiation with respect to ψ .

The principal stretches λ_1 and λ_2 in the meridian and circumferential directions indicate the degree to which the membrane is stretched at a given point. A value > 1 indicates stretching while < 1 means compression of the membrane. The relation between the prin-

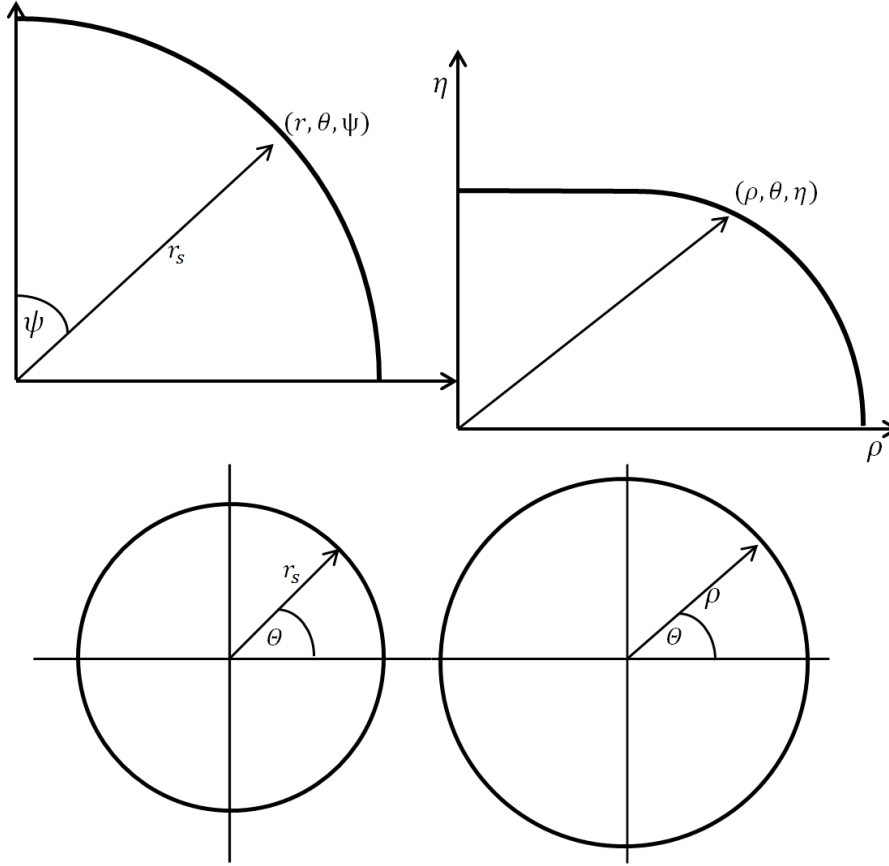


Figure 6: *Coordinate System*

cipal stretches and the coordinates is given by

$$\lambda_1 = \frac{dS}{ds} = \frac{1}{r_0}(\rho'^2 + \eta'^2)^{1/2}$$

$$\lambda_2 = \frac{\rho}{r_0 \sin\psi}$$

The equilibrium equations for membranes of revolution in the meridian tangential and normal directions are, from eqn (13) in Feng and Yang [12]:

$$\frac{dT_1}{d\rho} + \frac{1}{\rho}(T_1 - T_2) = \frac{P_t(r)}{\cos\theta} \quad (6)$$

$$K_1 T_1 + K_2 T_2 = P_n(r) \quad (7)$$

where P_n and P_t are the external loads acting on the deformed surface in the normal and tangential direction and T_1 and T_2 are the stress resultants. The relation between the stress resultants and the principal stretch ratios comes from the constitutive relation.

We assume that $P_t(r) = 0$ as force is only exerted by the top plate that is stationary with respect to the capsule. $P_n(r) = P$, where P is related to the volume of the deformed membrane. Thus we can rewrite these equation as

$$\left(\frac{\partial T_1}{\partial \lambda_1} \frac{\partial \lambda_1}{\partial \psi} + \frac{\partial T_1}{\partial \lambda_2} \frac{\partial \lambda_2}{\partial \psi} \right) \frac{\partial \psi}{\partial \rho} + \frac{1}{\rho}(T_1 - T_2) = 0 \quad (8)$$

$$K_1 T_1 + K_2 T_2 = P \quad (9)$$

where K_1 and K_2 are the principal curvatures in the deformed configuration.

Contact Region In the contact region we have that $\eta' = 0$ and hence the principal stretch ratios reduce to

$$\lambda_1 = \frac{\rho'}{r_0} \quad (10)$$

$$\lambda_2 = \frac{\rho}{r_0 \sin(\psi)} \quad (11)$$

Differentiating the expression for λ_2 with respect of ψ we find that

$$\lambda_2' = \frac{\lambda_1 - \lambda_2 \cos(\psi)}{\sin(\psi)} \quad (12)$$

Turning our attention to equations 8 and 9, we see that the second equation, for normal pressure, is automatically satisfied as $K_1 = K_2 = 0$. For convenience, the relations between the tension and the stretch, which are determined by the constitutive law, are written in terms of functions f_1 , f_2 and f_3

$$f_1 = \frac{\partial T_1}{\partial \lambda_1} \quad ; \quad f_2 = \frac{\partial T_1}{\partial \lambda_2} \quad ; \quad f_3 = T_1 - T_2 \quad (13)$$

Assuming that $P_t(r) = 0$ we can rearrange the first equation:

$$\lambda_1' = -\lambda_2' \frac{f_2}{f_1} + \frac{\rho'}{\rho} \frac{f_3}{f_1}$$

$$\lambda_1' = -\frac{\lambda_1 - \lambda_2 \cos \psi}{\sin \psi} \frac{f_2}{f_1} + \frac{\lambda_1}{\lambda_2 \sin \psi} \frac{f_3}{f_1}$$

Non-Contact Region In the non-contact region, it is convenient to write the equations of λ_2 in terms of $\delta = \lambda_2 \sin(\psi)$. The rate of change of δ with respect to ψ is assigned the symbol $\omega = \delta'$. We rearrange the first equation 8 to leave only λ_1' on the left hand side:

$$\lambda_1' = -\lambda_2' \left(\frac{f_2}{f_1} \right) + \frac{\rho'}{\rho} \left(\frac{f_3}{f_1} \right)$$

$$\lambda_1' = -\frac{\omega \sin \psi - \delta \cos \psi}{\sin^2 \psi} \left(\frac{f_2}{f_1} \right) + \frac{\omega}{\delta} \left(\frac{f_3}{f_1} \right)$$

Now let us consider the equation 9. The principle curvatures are

$$k_1 = \frac{d\theta}{dS}; \quad k_2 = \frac{\sin \theta}{\rho} \quad (14)$$

where the angle θ is the angle measured from the positive axis of symmetry to the outward normal of the deformed membrane surface and can be related to the deformed surface by

$$\cos \theta = \frac{d\rho}{dS}; \quad \sin \theta = -\frac{d\eta}{dS} \quad (15)$$

We can now express the curvatures in terms of deformed and undeformed coordinates

$$k_1 = \frac{\rho' \eta'' - \eta' \rho''}{(d\rho^2 + d\eta^2)^{3/2}}; \quad k_2 = \frac{-\eta'}{\rho(d\rho^2 + d\eta^2)^{1/2}} \quad (16)$$

Using the relations for the principle stretches (10) (11), we can write the principal curvatures K_1 and K_2 in terms of these

$$K_1 = \frac{1}{r_0 \sqrt{\lambda_1^2 - \delta'^2}} \left(\frac{\lambda_1' \omega}{\lambda_1^2} - \frac{\omega'}{\lambda_1} \right) \quad (17)$$

$$K_2 = \frac{1}{r_0 \lambda_1 \delta} \sqrt{\lambda_1^2 - \omega^2} \quad (18)$$

we can rewrite eqn 9 as

$$\begin{aligned} \frac{1}{r_0 \sqrt{\lambda_1^2 - \omega^2}} \left(\frac{\lambda_1' \omega}{\lambda_1^2} - \frac{\omega'}{\lambda_1} \right) T_1 + \frac{1}{r_0 \lambda_1 \delta} \sqrt{\lambda_1^2 - \omega^2} T_2 &= P \\ \left(\frac{\omega'}{\lambda_1} - \frac{\lambda_1' \omega}{\lambda_1^2} \right) T_1 &= \frac{(\lambda_1^2 - \omega^2) T_2}{\lambda_1 \delta} - \sqrt{\lambda_1^2 - \omega^2} P r_0 \\ \omega' &= \frac{\lambda_1' \omega}{\lambda_1} + \frac{(\lambda_1^2 - \omega^2) T_2}{\delta T_1} - \frac{\lambda_1 (\lambda_1^2 - \omega^2)^{\frac{1}{2}} P r_0}{T_1} \end{aligned} \quad (19)$$

In summary, for the contact region we have

$$\frac{\partial \lambda_1}{\partial \psi} = \frac{\lambda_1}{\lambda_2 \sin \psi} \begin{pmatrix} f_3 \\ f_1 \end{pmatrix} - \begin{pmatrix} \lambda_1 - \lambda_2 \cos \psi \\ \sin \psi \end{pmatrix} \begin{pmatrix} f_2 \\ f_1 \end{pmatrix} \quad (20)$$

$$\frac{\partial \lambda_2}{\partial \psi} = \frac{\lambda_1 - \lambda_2 \cos \psi}{\sin \psi} \quad (21)$$

In the non-contact region, it is convenient to write the equations of λ_2 in terms of $\delta = \lambda_2 \sin(\psi)$. The rate of change of δ with respect to ψ is assigned the symbol ω .

$$\frac{\partial \lambda_1}{\partial \psi} = - \left(\frac{\delta \cos \psi - \omega \sin \psi}{\sin^2 \psi} \right) \begin{pmatrix} f_2 \\ f_1 \end{pmatrix} + \left(\frac{\omega}{\delta} \right) \begin{pmatrix} f_3 \\ f_1 \end{pmatrix} \quad (22)$$

$$\frac{\partial \delta}{\partial \psi} = \omega \quad (23)$$

$$\frac{\partial \omega}{\partial \psi} = \frac{\lambda_1' \omega}{\lambda_1} + \frac{\lambda_1^2 - \omega^2}{\delta} \frac{T_2}{T_1} - \frac{\lambda_1 (\lambda_1^2 - \omega^2)^{1/2} P r_0}{T_1} \quad (24)$$

The constitutive law determines the functions $f_1 - f_3$, specifically

$$f_1 = \frac{\partial T_1}{\partial \lambda_1} \quad ; \quad f_2 = \frac{\partial T_1}{\partial \lambda_2} \quad ; \quad f_3 = T_1 - T_2 \quad (25)$$

There are 5 boundary conditions. At the pole, where $\psi = 0$, $\lambda_1 = \lambda_2$ due to the rotational symmetry of the problem. At the border between the contact and non-contact region ($\psi = \Gamma$), λ_1 and λ_2 must be continuous as well as $\delta' = \lambda_1$ from equation 21. Finally, at the equator ($\psi = \pi/2$) ω must be zero.

$$\psi = 0 : \quad \lambda_1 = \lambda_2 = \lambda_0 \quad (26)$$

$$\psi = \Gamma : \quad \eta' = 0 \quad \text{or} \quad \delta' = \lambda_1 \quad (27)$$

$$\psi = \Gamma : \quad (\lambda_1)_{\text{contact}} = (\lambda_1)_{\text{non-contact}} \quad (28)$$

$$\psi = \Gamma : \quad (\lambda_2)_{\text{contact}} = (\lambda_2)_{\text{non-contact}} \quad (29)$$

$$\psi = \frac{\pi}{2} : \quad \delta' = 0 \quad (30)$$

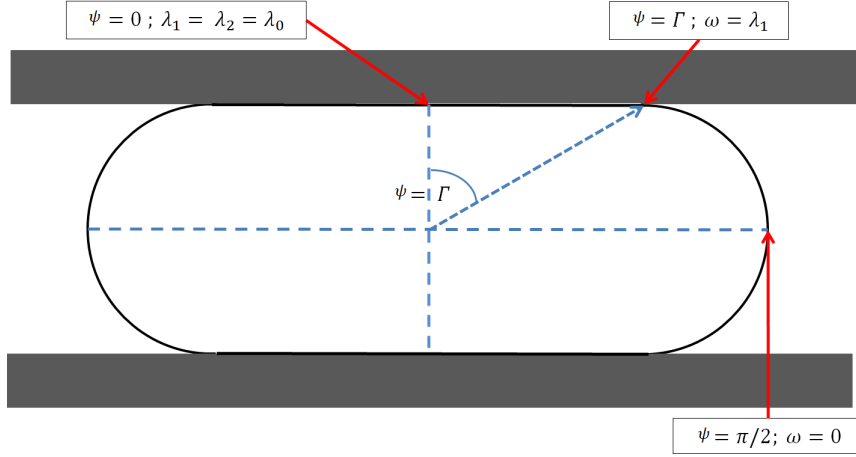


Figure 7: Sketch of the compression of a capsule between parallel plates. Only one quadrant is considered in the numerical scheme.

These boundary conditions are indicated in Fig. 7.

The volume of the inflated membrane after contact can be found

$$V = 2\pi r_0^3 \int_{\Gamma}^{\frac{\pi}{2}} (\lambda_1^2 - \delta'^2)^{1/2} \delta^2 d\psi \quad (31)$$

and hence the pressure P after contact, where the initial pressure P_0 depends on the constitutive law. Here T is the tension when $\lambda_1 = \lambda_2 = \lambda$ and λ_s is the pre-inflation, specifying that the radius of the capsule increased from r to $\lambda_s r$.

$$P = \frac{2P_0\lambda_s^3}{3 \int_{\Gamma}^{\frac{\pi}{2}} (\lambda_1^2 - \omega^2)^{\frac{1}{2}} \delta^2 d\psi} \quad \text{where} \quad P_0 = \frac{2T(G_s, \lambda_s)}{\lambda_s r_0} \quad (32)$$

3.2.3 Constitutive Equation

To determine the functions $f_1 - f_3$ a constitutive law for the material properties is needed. We will consider three constitutive law, all assuming a two dimensional membrane. The equation for T_1 is given. The form of T_2 can be found by interchanging the indices 1 and 2.

Neo-Hookian Model

The Neo-Hookian model assumes the membrane is a incompressible, thin isotropic material. This constitutive law is strain softening:

$$T_1 = \frac{G_s}{\lambda_1 \lambda_2} \left(\lambda_1^2 - \frac{1}{(\lambda_1 \lambda_2)^2} \right) \quad (33)$$

where G_s is the surface shear elastic modulus.

Skalak law

The Skalak law was original developed by Skalak *et al* [46] to descrieb the almost area-incompressible membrane of red blood cells and is strain-hardening:

$$T_1 = G_s \left(\frac{\lambda_1}{\lambda_2} (\lambda_1^2 - 1) + C \lambda_1 \lambda_2 ((\lambda_1 \lambda_2)^2 - 1) \right) \quad (34)$$

The first term describes the effect of shear deformation with a surface shear elastic modulus G_s . The second term accounts for area dilation with a modulus of $C G_s$. In its original

formulation for red blood cells the constant C was large to make for a material that is easily sheared and almost area-incompressible. However, the law is general and can be applied to membranes that are area compressible by lowering the value of C .

Evans and Skalak Law

Proposed by Evans and Skalak [47] to model biological membranes.

$$T_1 = G_s \left(\frac{\lambda_1^2 - \lambda_2^2}{2\lambda_1^2\lambda_2^2} + A(\lambda_1\lambda_2 - 1) \right) \quad (35)$$

The shear deformation is characterised by the first term with a modulus G_s . The second term accounts for area dilation with a modulus $A G_s$. For membranes that are almost area-incompressible the parameter A is large.

3.2.4 Numerical Implementation

Feng and Yang implemented a shooting method for the solution of these equations. After duplicating this implementation in Python and finding it sensitive to the initial conditions and liable not to converge, this approach was abandoned.

Instead, the problem was implemented using a first order finite difference method in MATLAB with the help of Draga Pihler-Puzovic.

To confirm the correctness of the model, the case of an inflated sphere with no compression was studied. In this case, the principal stretches should be constant and equal to the pre-inflation λ_s . For small numbers of grid points $N = 50$, the principal stretches deviate up to 1.5 % from the expected value. As the number of grid points is increased, the error is reduced proportional to $h = 2\pi/N$, the grid spacing. For $N = 1600$, the deviation of from λ_s is less than 0.07 %. This is illustrated in Figure 8.

We draw the conclusion that for $N = 200$ we can expect the error in the principal stretches to be below 1 %. To test the validity of the full model, the case of minor compression was used. Results reported in the literature indicate that as the compression increases, the stretches gradually depart from being constant throughout the membrane. They are reduced in the region in contact with the plate, which leads to the formation of a dimple in the absence of preinflation. The stretches in the non-contact region increase.

However, the results with the current code do not produce this expected results. Given the possible existence of multiple solutions, several approaches were taken. Different starting guesses were supplied. However, the modification always lead to the convergence to the original solution, as shown in Figure 9 a). An alternative solution was finally found by modifying the solution such that the principle stretches are equal to the preinflation but ω is left unchanged.

Current work is focused on finding all solutions to the equations. Additionally, here are two possible sources of error. One one hand, the governing equations used could be wrong, given the disagreement in the literature over the exact form. A summary of the reported equations is given in the Appendix. On the other hand, an error in the implementation could be the cause.

As the output of interest is not the principal stretches but the shear modulus G_s , the question of its sensitivity to the grid size warrants future investigation. This investigation will be repeated once the full model has been validated. Additionally to the grid size, the effect of the constitutive law was investigated by comparing the Neo-Hookian and the Skalak model with $C = 0$.

The resulting shear modulus for two cases case $((\Gamma, P) = (43^\circ, 224)$ and $(73^\circ, 1410))$ at three different preinflations ($\lambda_s = 1.05, 1.1, 1.2$) are shown in Figure 10. It is apparent

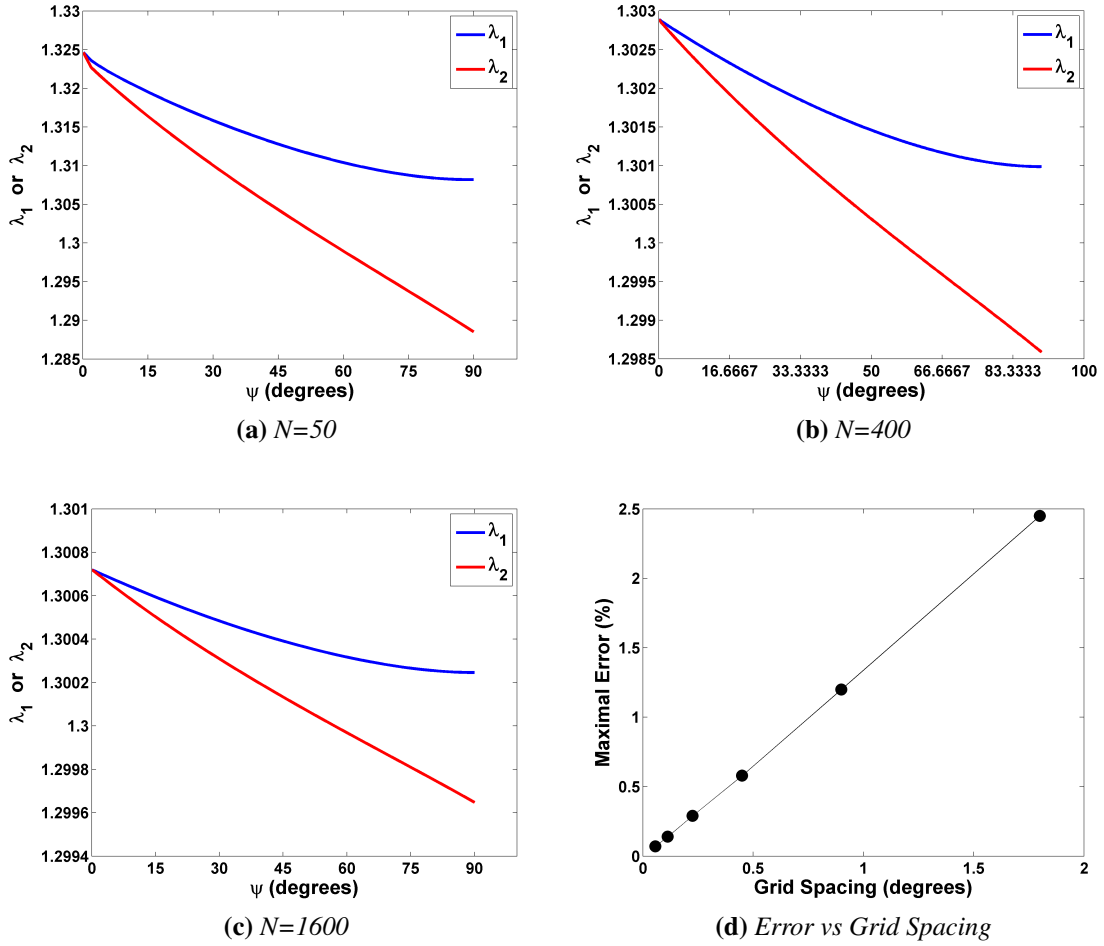


Figure 8: The principal stretch ratios in the meridian λ_1 and circumferential λ_2 direction for the case of no compression (i.e. $\Gamma = 0$) and a preinflation of 30 % ($\lambda_s = 1.3$) with a Neo-Hookian law. The graphs show the results for varying numbers of grid points N **a)** $N=50$ **b)** $N=400$ **c)** $N=1600$ **d)** Maximal error versus the grid spacing h ($= 1/N$). The error decreases proportional to the grid spacing as expected when using a first order method.

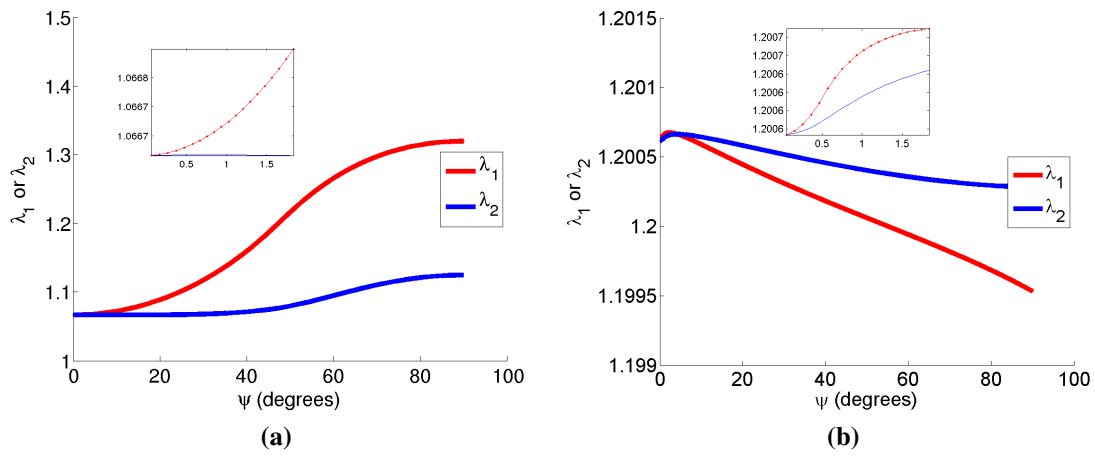


Figure 9: The principal stretch ratios in the meridian λ_1 and circumferential λ_2 direction for the case of small compression (i.e. $\Gamma = 0.01$) and a preinflation of 20 % ($\lambda_s = 1.2$) with a Neo-Hookian law. Inserts show transition between contact and non-contact region at 0.6° . **a)** Typical Result **b)** Alternative solution when stretch ratios are set equal to the preinflation but ω is left unchanged. Note the difference in scale of the y-axis.

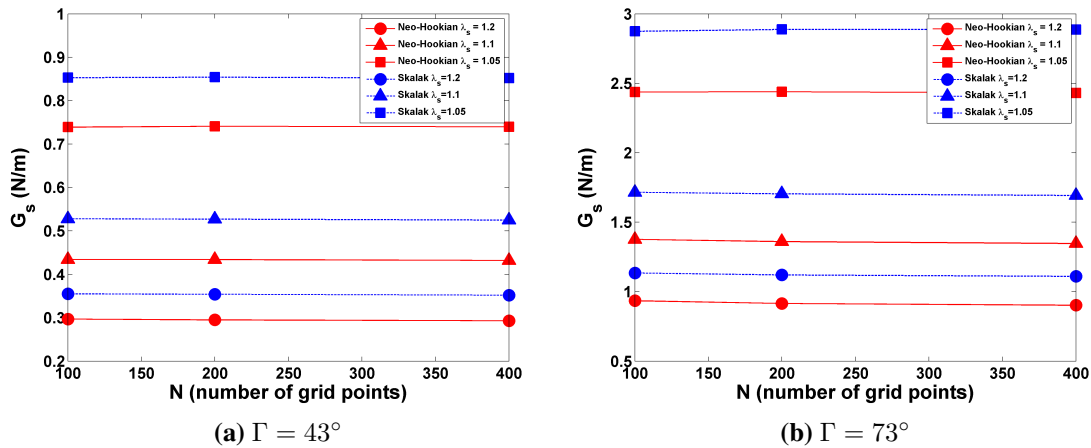


Figure 10: Effect of grid size, preinflation and constitutive law on the value of the area shear modulus G_s . The red symbols are calculated with the Neo-Hookian law and blue symbols with the Skalak law. Circles correspond to $\lambda_s = 1.2$, triangles to $\lambda_s = 1.1$ and squares to $\lambda_s = 1.05$. For $N \geq 100$ the grid size does not affect the shear modulus. **a)** At moderate compression with $\Gamma = 43^\circ$. **b)** At large compression with $\Gamma = 73^\circ$.

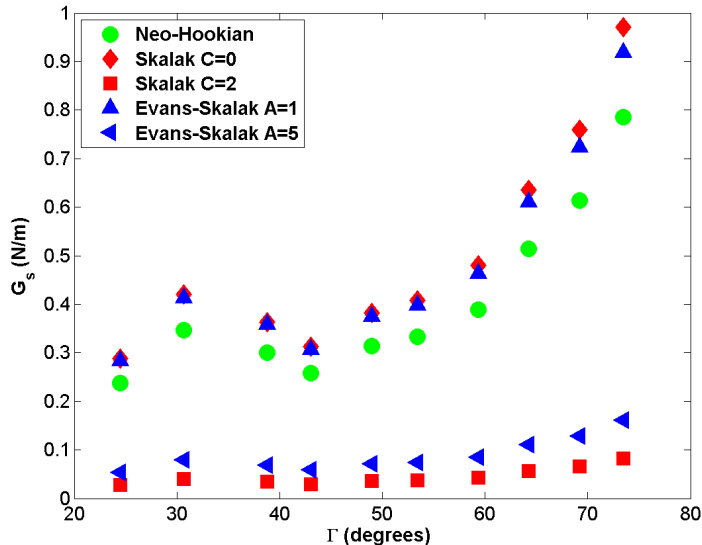


Figure 11: Resulting surface shear modulus for a capsule being compressed with different constitutive laws. The capsule membrane appears to be strain-hardening. However, no conclusions can be drawn until the code has been fully validated.

that the value of G_s is independent of grid size for $N \geq 100$. It also can be seen that the effect of the constitutive law, while not unimportant, is outweighed by the effect of a 5 % change in preinflation.

An example of results is given in Figure 11 based on the compression of a capsule made with 0.002 molar NaOH. It can be seen that this method allows for a clear distinction of different constitutive laws, given compression data. The large deviation at low compression is due to variations in the pressure determined from experiments.

3.3 Compression in a Pipette

We have found that the compression between rigid plates offers the best measurement technique that can be implemented without extensive simulations. However, the dependence on sophisticated compression equipment and relative difficulty of carrying out accurate measurements means there is room for improvement.

We have been inspired by the work of Wyss *et al* [20] who determined the linear elastic response of gel beads pressed into the conical tip of a pipette under a known pressure, see Figure 12 for an illustration. A limitation is the restriction to small deformation as our capsule routinely undergoes extensions of 100 % or more in the flow.

3.3.1 Wyss *et al* Pipette Method

A short outline of the formalism will be given here, the full argument can be found in Wyss *et al* paper. In equilibrium, the stress applied to the capsule must be balanced by the elastic forces. We take the central axis of the capillary to be the z -direction of a cylindrical coordinate system.

The stresses in the longitudinal direction of the capillary must be equal to the applied pressure difference $\sigma_z = p$. In the absence of static friction, the longitudinal component of the wall force must exactly balance the applied pressure difference. Given that the wall of the capillary makes an angle α with the z -axis the force acting on the surface